



Quarterly peer-reviewed scientific journal

ISSN 1505-4675
e-ISSN 2083-4527

TECHNICAL SCIENCES

Homepage: www.uwm.edu.pl/techsci/



DOI: <https://doi.org/10.31648/ts.6087>

INVESTIGATION OF LOW- AND HIGH-CYCLE FATIGUE IN AL 2024-T4 ALLOY

Sylwester Kłysz

ORCID: 0000-0002-4521-4972
Department of Technical Sciences
University of Warmia and Mazury in Olsztyn
Airworthiness Division
Air Force Institute of Technology in Warsaw

Received 6 November 2020, accepted 5 January 2021, available online 5 January 2021.

Key words: low-cycle fatigue, high-cycle fatigue, 2024 aluminum alloy, Manson-Coffin equation, Morrow equation, S-N curves.

Summary

The article presents the results of low- (LCF) and high-cycle fatigue (HCF) analyses of 2024-T4 aluminum alloy which is used in aircraft construction, mainly for highly loaded structural components, including for plating, fuselage frames and rotor blade girders in helicopters. The alloy is used in structures where a high strength-to-weight ratio and high fatigue resistance are required. However, the alloy is poorly weldable and has low corrosion resistance.

The tests were performed on hourglass and cylindrical samples with parallel and perpendicular orientation relative to the rolling direction. Samples for analysis were obtained from the production line of PZL-130 Orlik TC-II trainer aircraft. The results of the analysis were described by Manson-Coffin and Morrow equations.

Correspondence: Sylwester Kłysz, Katedra Mechaniki i Podstaw Konstrukcji Maszyn, Wydział Nauk Technicznych, Uniwersytet Warmińsko-Mazurski, ul. M. Oczapowskiego 11, 10-719 Olsztyn, e-mail: sylwester_k@uwm.edu.pl

Introduction

Aluminum alloys are widely applied in civilian and military engineering (HEINZ et al. 2000, PETRASEK et al. 2013, *Problemy badań i eksploatacji...* 1993). They are used in the production of the structural components of aircraft, including plating, fuselage frames, stringers and hatches. The EN AW-2024 T4 aluminum alloy is used in highly loaded structural components and plating where a high strength-to-weight ratio and high fatigue resistance are required. However, the alloy is poorly weldable and has low corrosion resistance.

Analyses of the performance of aircraft structures indicate that mechanical strain is the main cause of damage to aviation plating (SIENIAWSKI 2002). Plating is damaged due to the initiation and propagation of cracks, and the material's strength is determined by the number of cycles until destruction within a given range of plastic or total strain values (NOGUEIRA et al. 2020, POLAK 1991). Analyses of materials' behavior under variable loads in a small number of cycles provide valuable information and support the identification of cyclic fatigue mechanisms, localization of strain, cracks and failure of structural components (LI et al. 2019, FENG, QIAN 2018, IGNATOVICH et al. 2013).

Analyses of low-cycle fatigue resistance are also helpful in estimating the service life of structural components. The shape of the hysteresis loop during low-cycle fatigue resistance tests and their stabilized dimensions are determined by the type of material and loading conditions. An extensive analysis of fatigue parameters and changes in the shape of the hysteresis loop under various experimental and operating conditions, and the extent to which changes in the properties of materials subjected to cyclic and variable loading (including overloading) affect fatigue resistance and the shape of the hysteresis loop was presented by (GOSS 1982, KŁYSZ 2000). The results of similar studies are found in the literature – however, in order to compare them with each other and apply them to specific analyzes, it is always necessary to take into account the correct composition, mechanical and temperature processing condition of the tested material – which is not always clearly documented. These tests were performed for the purpose of introducing own material characteristics to the FEM strength analyzes of elements made of materials taken directly from the production line of the PZL-130 Orlik TC-II aircraft.

The aim of this study was to describe low- and high-cycle fatigue of hourglass and cylindrical samples of 2024-T4 alloy with the use of Manson-Coffin and Morrow equations. The alloy's fatigue resistance was evaluated in samples with parallel and perpendicular orientation relative to the sheet rolling direction. The results were analyzed by calculating the parameters of Manson-Coffin and Morrow equations as well as the equations presented by the U.S. Department of Transportation of the Federal Aviation Administration (DOT/FAA/AR-MMPDS-01... 2003).

Materials and Methods

The experiment involved hourglass and cylindrical samples with a diameter of $\varnothing 6.5$ mm (Fig. 1). The samples were obtained from the production line of PZL-130 Orlik TC-II trainer aircraft in the following configuration:

- parallel to the rolling direction, (longitudinal samples, T-L orientation),
- perpendicular to the rolling direction, (transverse samples, L-T orientation).

The chemical composition of 2024-T4 alloy based on standard PN-EN 573-3 is presented in Table 1. The mechanical properties of the analyzed alloy are presented in Table 2 according to Standard PN-EN 485-2, in Table 3 according to the specifications of ASM Aerospace Specification Metals Inc., and in Tables 4 and 5 according to MIL-HDBK-5J specifications.

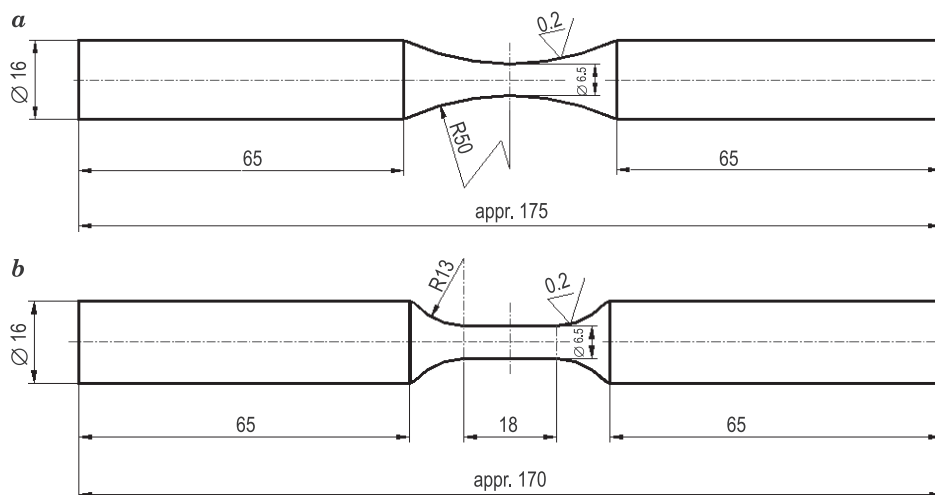


Fig. 1. Shape and dimensions of samples for low- (a) and high-cycle (b) fatigue tests

Table 1

Chemical composition [%] of EN AW-2024 T4 alloy to Standard PN-EN 573-3: 2009

Si	Fe	Cu	Mn	Mg	Cr	Zn	Ti	Other	Al
0.50	0.50	3.8-4.9	0.30-0.9	1.2-1.8	0.10	0.25	0.15	0.15	other

Source: PN-EN 573-3: *Aluminium i stopy aluminium – Skład chemiczny i rodzaje wyrobów przerobionych plastycznie. Część 3: Skład chemiczny i rodzaje wyrobów* (2009).

Table 2

Mechanical properties of EN AW-2024 T4 alloy acc. to Standard PN-EN 485-2: 2009

R_m [MPa]	R_e [MPa]	$A_{50\text{ mm}}$ [%]	HBW
min. 425	min. 275	min. 14	120

Source: PN-EN 485-2: *Aluminium i stopy aluminium – Blachy, taśmy i płyty. Część 2: Własności mechaniczne* (2009).

Table 3

Mechanical properties of 2024 T4 and 2024 T351 alloys acc. to ASM

R_m^* [MPa]	R_e^* [MPa]	A^* [%]	E^* [GPa]	ν	K_{1C} [MPa $\sqrt{\text{m}}$]	Z^* [MPa]	HB*
2024 T4 and 2024 T351							
469	324	19 ($\varnothing = 12.5\text{ mm}$)	73.1	0.33	26 (S-L orientation)	138 (500,000,000 cycles; RR Moore)	120
		20 ($t = 1.6\text{ mm}$)			32 (T-L orientation)		
					37 (L-T orientation)		
2024 T3**							
483	345	18 ($t = 1.6\text{ mm}$)	73.1	0.33	–	138 (500,000,000 cycles; RR Moore)	120

* according to the ASM website, these data were provided by Aluminum Association Inc. and are not for design;

** according to the ASM website, these data were provided by Alcoa and are not for design.

Source: ASM Aerospace Specification Metals Inc. <http://asm.matweb.com>.

Table 4

Mechanical properties of 2024 T4 alloy (rolled bars) acc. to MIL-HDBK-5J

$R_{m, \text{ min}}$ [MPa]	$R_{e, \text{ min}}$ [MPa]	$A_{\text{ min}}$ [%]	E [GPa]	ν
	310 (L orientation) ¹	15 ³		
427 (L orientation) ¹	310 (L-T orientation) ¹	12 ⁴	72.4 ⁶	0.33
420 (L-T orientation) ¹	290 (L orientation) ²	8 ⁵	73.8 ⁷	
	290 (L-T orientation) ²			

Note: according to (SIENIAWSKI 2002), sample T4 is outdated and should not be used in newly designed structures:

¹ for rolled bars 3,175-25, 4 mm,

² for rolled bars 12,7-25,4 mm,

³ for sheets and plates with a thickness of 0.53-6.32 mm, L-T orientation,

⁴ for sheets and plates with a thickness of 6.35-12.675 mm, L-T orientation,

⁵ for sheets and plates with a thickness of 12.7-25.4 mm, L-T orientation,

⁶ for sheets and plates with a thickness of 0.254-6.32 mm,

⁷ for sheets and plates with a thickness of $\geq 6.35\text{ mm}$.

Source: MIL-HDBK-5J (2003).

Table 5

Mechanical properties of 2024 T3 alloy (sheets thickness of 0.25÷3.25) acc. to MIL-HDBK-5J

$R_{m, \min}$ [MPa]	$R_{e, \min}$ [MPa]	A_{\min} [%]	E [GPa]	ν
448 (L orientation)	331 (L orientation)	12	72.4	0.33
441 (L-T orientation)	296 (L-T orientation)	(L-T orientation)	(L-T orientation)	

Note: the presented values of R_m , R_e , A_{\min} , E and ν can be used for designing structural components of military aircraft, naval vessels and FAA aircraft.

Source: MIL-HDBK-5J (2003).

The low-cycle fatigue life of the examined samples was analyzed by determining fatigue durability (N_f) as a function of transverse strain ($\varepsilon_{\text{trans}}$) amplitude in the MTS 370.10 load frame with the MTS 632.18-F20 (measurement range 50 kN), cross-sectional strain extensometer (measurement range $\pm 2\%$). Loading frequency ranged from 0.05 Hz to 1 Hz.

The high-cycle fatigue of the samples was analyzed by determining fatigue durability (N_f) as a function of stress (σ_a) amplitude. The tests were carried out at a load frequency ranging from 15 Hz to 45 Hz.

Sampling rate 200 points/cycle. The tests were performed at room temperature, in the accredited Materials Testing Laboratory of the Air Force Institute of Technology. The test stands are presented in Figure 2.



Fig. 2. Samples analyzed in MTS 810.23 load frame with a cross-sectional strain extensometer

Analysis of low-cycle fatigue

The initial and middle (corresponding to approximately half the number of load cycles to failure) hysteresis loops were determined in each test, and the initial and stabilized values (accounting for the strengthening of the material under cyclic loading) of test parameters were determined for further analyses. Examples of stabilized hysteresis loops for transverse and longitudinal samples are presented in Figure 3.

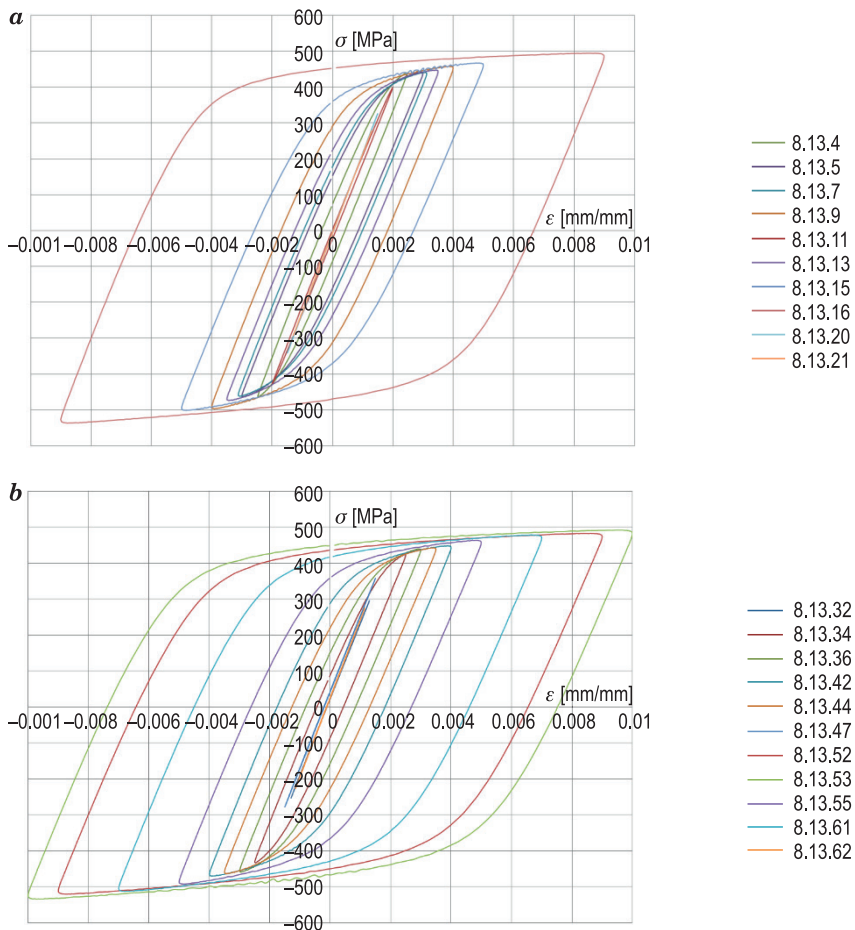


Fig. 3. Hysteresis loops: *a* – transverse samples, *b* – longitudinal samples

The Manson-Coffin relationship and coefficients were determined with the use of the following equation:

$$\frac{\Delta\varepsilon}{2} = \frac{\Delta\varepsilon_e}{2} + \frac{\Delta\varepsilon_{pl}}{2} = \varepsilon_f(2N_f)^a + \sigma_f(2N_f)^b \quad (1)$$

where:

$\varepsilon_{trans} = f(N_f)$, for data corresponding to the first and middle hysteresis loops (Fig. 4 and Fig. 5),

$2N_T$ and ε_T – coordinates of the point of intersection of lines $\varepsilon_e - 2N_f$ and $\varepsilon_{pl} - 2N_f$

The least squares method was used for individual components of deformation (elastic and plastic). The applied transverse strain ϵ_{trans} was converted to longitudinal strain ϵ_{long} with the use of the following formulas:

$$\epsilon = \epsilon_e + \epsilon_{pl}, \quad \epsilon_{long,e} = \frac{1}{\nu} \epsilon_{trans,e}, \quad \epsilon_{trans,pl} = \frac{1}{0.5} \epsilon_{trans,pl} \quad (2)$$

where ν is Poisson's ratio for stresses within the elastic range.

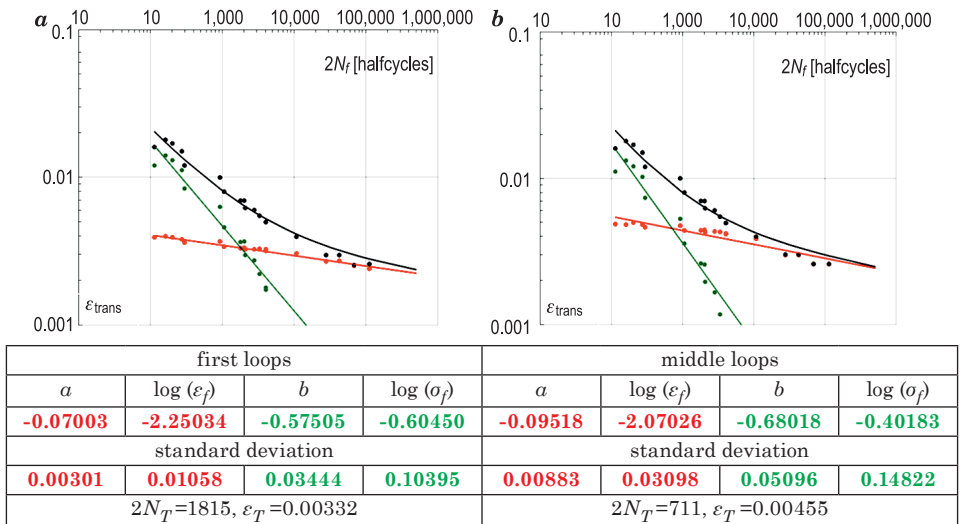


Fig. 4. Manson-Coffin curves for low-cycle fatigue data in the first (a) and middle (b) hysteresis loops in each test (transverse strain) – transverse samples

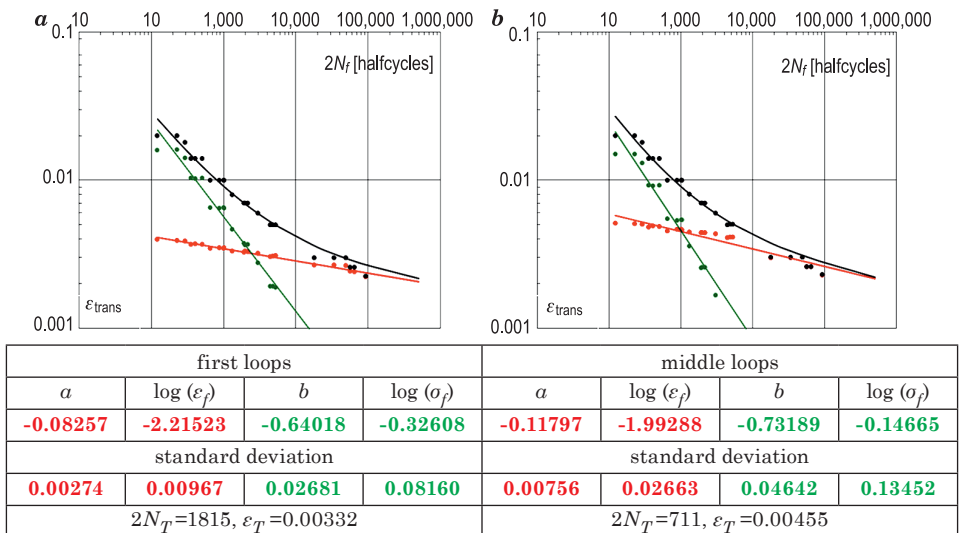


Fig. 5. Manson-Coffin curves for low-cycle fatigue data in the first (a) and middle (b) hysteresis loops in each test (transverse strain) – longitudinal samples

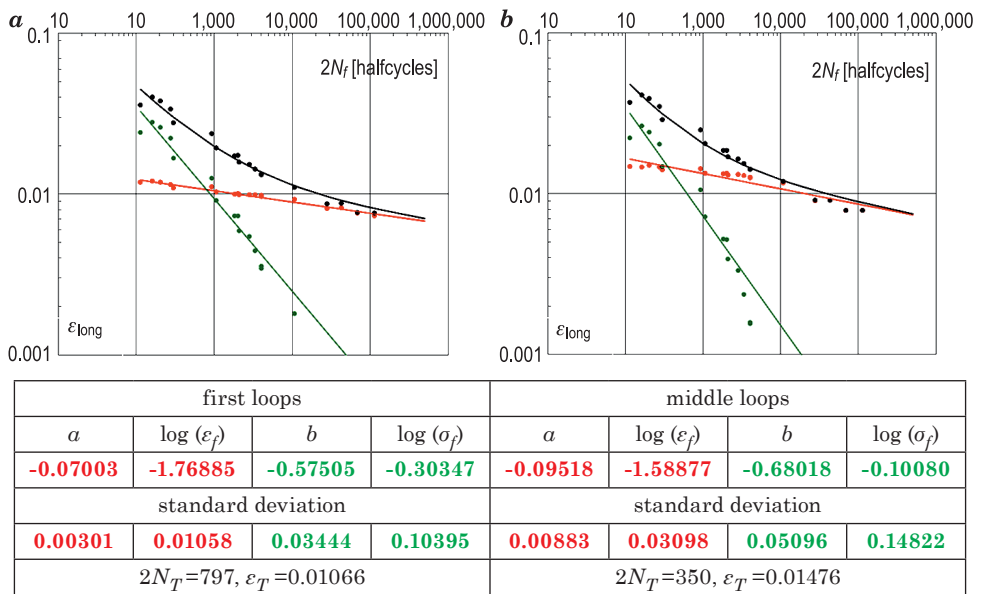


Fig. 6. Manson-Coffin curves for low-cycle fatigue data in the first (a) and middle (b) hysteresis loops in each test (longitudinal strain) – transverse samples

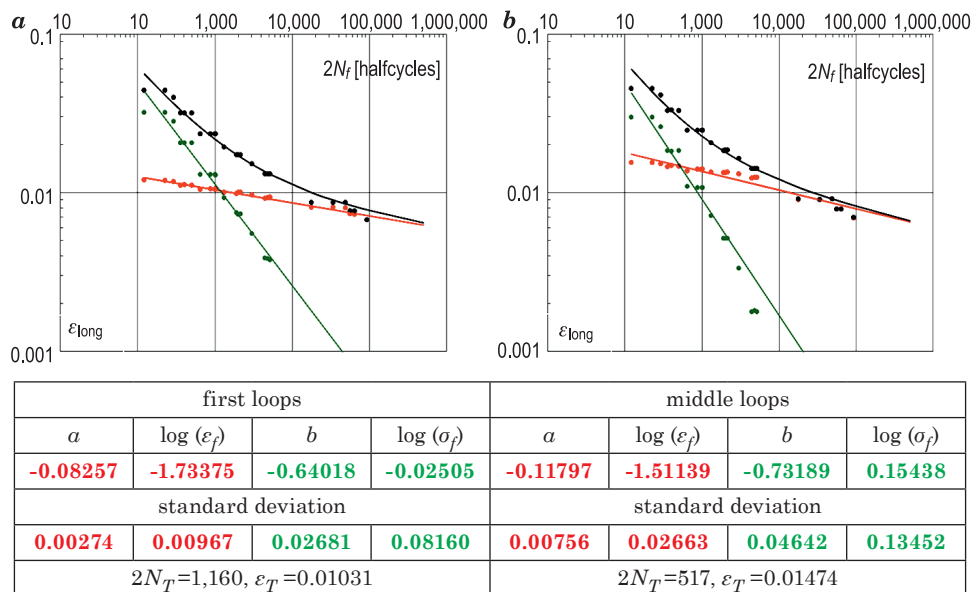


Fig. 7. Manson-Coffin curves for low-cycle fatigue data in the first (a) and middle (b) hysteresis loops in each test (longitudinal strain) – longitudinal samples

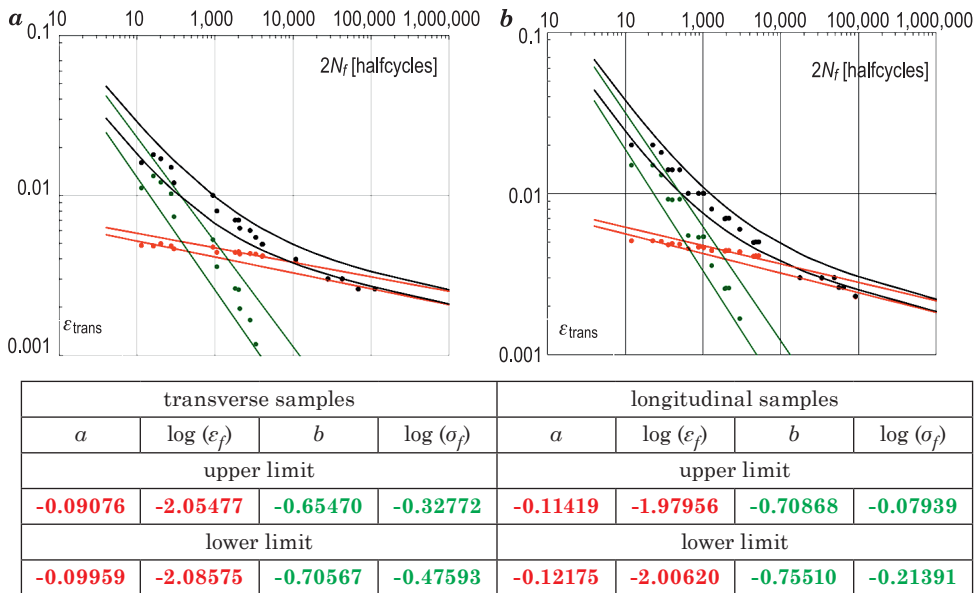


Fig. 8. Manson-Coffin curves – fatigue limits in low-cycle fatigue curves for middle hysteresis loops in each test – transverse strain

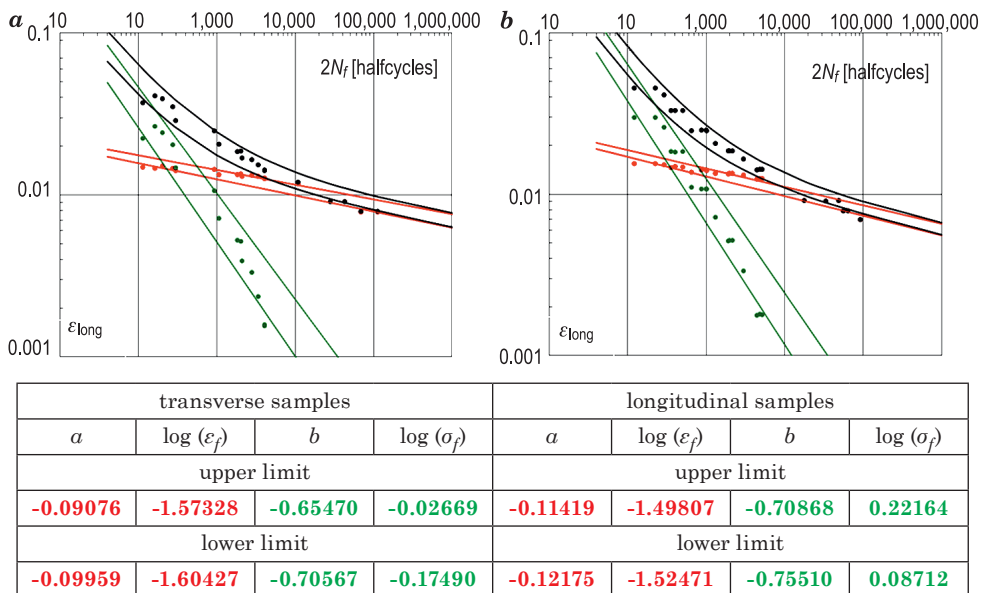


Fig. 9. Manson-Coffin curves – fatigue limits in low-cycle fatigue curves for middle hysteresis loops in each test – longitudinal strain

Manson-Coffin relationships and coefficients at $\epsilon_{\text{long}} = f(N_f)$ were determined for the data corresponding to the first and middle hysteresis loops (Fig. 6 and Fig. 7).

Manson-Coffin relationships and coefficients at coordinates $\epsilon_{\text{trans}} = f(N_f)$ and $\epsilon_{\text{long}} = f(N_f)$ were determined for the data corresponding to the middle hysteresis loops as the lower and upper limits of fatigue relative to the relationships shown in Figures 4b, 5b, 6b and 7b. The width of the fatigue limit was determined based on the standard deviation of each coefficient in the Manson-Coffin equation (Fig. 8 and Fig. 9).

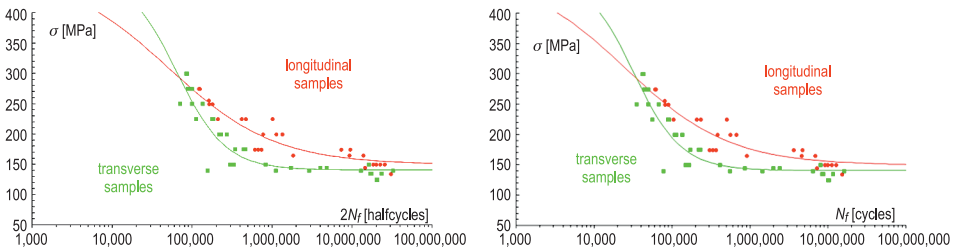
Analysis of high-cycle fatigue

The high-cycle fatigue of the examined samples was analyzed for stress curves $\sigma = f(N)$:

– The equations and the coefficients were determined with the use of formula (3) (KŁYSZ et al. 2010):

$$\sigma_a = \text{Be} \left(\frac{1}{\left(\frac{2N_f}{E} \right)^D + c} \right) \tag{3}$$

in two variants: $\sigma = f(2N_f)$ (as a function of the number of half-cycles) and $\sigma = f(N_f)$ (as a function on the number of cycles). The resulting curves and coefficients are presented in Figure 10.



	transverse samples		longitudinal samples	
	$\sigma = f(2N_f)$	$\sigma = f(N_f)$	$\sigma = f(2N_f)$	$\sigma = f(N_f)$
$A =$	636.32	246.13	23.90	15.42
$B =$	140.55	140.55	149.03	149.03
$C =$	531.01	205.39	20.83	13.44
$D =$	1.3705	1.3705	0.6321	0.6321
$E =$	1,000	1,000	1,000	1,000

Fig. 10. Stress $\sigma = f(N)$ calculated with formula (3) for transverse and longitudinal samples of 2024 T4 alloy

– The equation and the coefficients were determined with the use of formula (4) (DOT/FAA/AR-MMPDS-01 2003):

$$\log(N_f) = A + B \log(S_{eq} - C) \tag{4}$$

$$S_{eq} = S_{max}(1 - R)^D$$

The resulting curves and coefficients are presented in Figure 11.

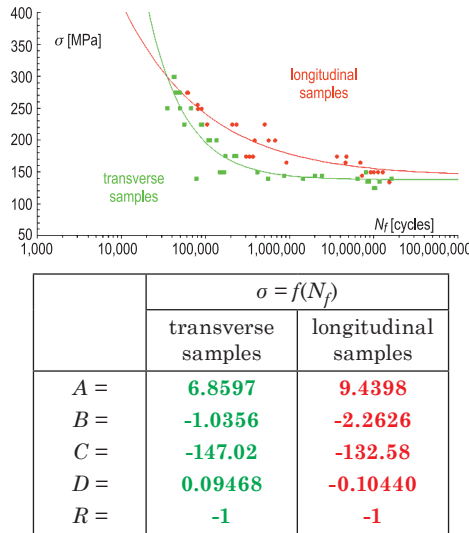


Fig. 11. Stress $\sigma = f(N_f)$ calculated with formula (4) for transverse and longitudinal samples of 2024 T4 alloy

The curves described by equations (3) and (4) are compared in Figure 12.

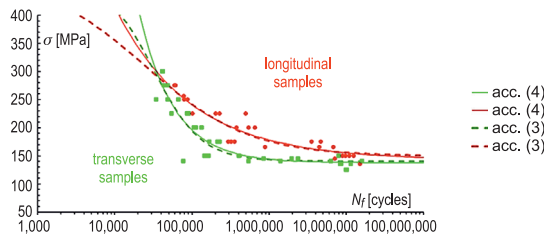


Fig. 12. Stress $\sigma = f(N_f)$ calculated with equations (3) and (4) for transverse and longitudinal samples of 2024 T4 alloy

Conclusions

A comparison of Manson-Coffin curves in low-cycle fatigue analyses demonstrates that transverse samples are characterized by somewhat longer low-cycle fatigue than longitudinal samples. The range of elastic strain components increases, and the range of plastic strain components decreases (coefficients ε_f and σ_f , respectively) during fatigue tests, which indicates that the rigidity of the examined samples decreases during tests. These changes are estimated at 10%.

The slope of Manson-Coffin curves (exponents a and b) increases with the cyclic stabilization of test conditions, which decreases the number of cycles and increases deformation at the point of curve intersection. These changes are estimated at 25-40%.

The above changes in Manson-Coffin coefficients occur regardless of sample type (longitudinal/transverse) or type of strain ($\varepsilon_{\text{trans}}/\varepsilon_{\text{long}}$); therefore, stabilized hysteresis loops can be predicted based on the first hysteresis loops. Since only two points are required to plot a line, Manson-Coffin curves can be correctly plotted when the low-cycle fatigue analysis is limited to only two extreme (or randomly selected) loads. However, this procedure requires further experimental verification and analysis.

The stabilized hysteresis loops are characterized by greater divergence than initial hysteresis loops. The above also leads to a greater scatter of fatigue limit values in the tested samples.

At $\varepsilon_{\text{trans}} = f(2N_f)$, the Manson-Coffin equation can be written in a conservative form based on the averaged values of the coefficients for the upper and lower fatigue limits:

$$\frac{\Delta\varepsilon}{2} = 0.0100 \cdot (2N_f)^{-0.1066} + 0.6620(2N_f)^{-0.7060} \quad (5)$$

and the optimistic version of the equation can be expressed by:

$$\frac{\Delta\varepsilon}{2} = 0.0085 \cdot (2N_f)^{-0.1066} + 0.3951(2N_f)^{-0.7060} \quad (6)$$

A comparison of Morrow curves for high-cycle analyses indicates that longitudinal samples are characterized by significantly longer high-cycle fatigue than transverse samples.

Stress curves $\sigma = f(N)$ described with equations (3) and (4) can be regarded as equivalent within the range of the experimental data. The relationship presented in formula (3) assumes a more realistic course when fatigue limits are lower or higher than those determined in this experiment.

References

- ASM Aerospace Specification Metals Inc. <http://asm.matweb.com>.
- DOT/FAA/AR-MMPDS-01. *Metallic Materials Properties*. 2003. Development and Standardization (MMPDS), U.S. Department of Transportation Federal Aviation Administration.
- FENG L, QIAN X. 2018. *Low cycle fatigue test and enhanced lifetime estimation of high strength steel S550 under different strain ratios*. Marine Structures, 61: 343–360.
- GOSS C. 1982. *Doświadczalna i teoretyczna analiza własności stali o podwyższonej wytrzymałości w zakresie małej liczby cykli obciążenia*. Biuletyn WAT, 11.
- HEINZ A., HASZLER A., KEIDEL C., MOLDENHAUER S., BENEDICTUS R., MILLER W. 2000. *Recent development in aluminium alloys for aerospace applications*. Material Sciences and Engineering A, 280: 102–107.
- IGNATOVICH S.R., MENOUE A., KARUSKEVICH M.V., MARUSCHAK P.O. 2013. *Fatigue damage and sensor development for aircraft structural health monitoring*. Theoretical and Applied Fracture Mechanics, 65: 23–27.
- KŁYSZ S. 2000. *Wpływ przeciążeń i sekwencji obciążeń na własności niskocyklowe stali 18G2A i St3SY*. Zagadnienia Eksploatacji Maszyn, 4(124): 139–154.
- KŁYSZ S., LISIECKI J., BĄKOWSKI T. 2010. *Modyfikacja równania do opisu krzywych Wöhlera*. Prace Naukowe ITWL, 27: 93–97.
- LI Y., RETRAINT D., XUE H., GAO T., SUN Z. 2019. *Fatigue properties and cracking mechanisms of a 7075 aluminum alloy under axial and torsional loadings*. Procedia Structural Integrity, 19: 637–644.
- MIL-HDBK-5J. *Department of Defense Handbook-Metallic Materials and Elements for Aerospace Vehicle Structures*. 2003.
- NOGUEIRA F., CUNHA J., MATEUS A., MALÇA C., COSTA J.D., BRANCO R. 2020. *Cyclic plastic behaviour of 7075 aluminium alloy*. 1st Virtual Conference on Structural Integrity – VCSI.1 Procedia Structural Integrity, 25: 438–444.
- PETRASEK M., IGNATOVICH S., KARUSKEVICH M., MASLAK T. 2013. *Surface of metal as an indicator of fatigue damage*. Advances in Military Technology, 8(2): 83–91.
- PN-EN 485-2: *Aluminium i stopy aluminium – Blachy, taśmy i płyty*. Część 2: *Własności mechaniczne*. 2009.
- PN-EN 573-3: *Aluminium i stopy aluminium – Skład chemiczny i rodzaje wyrobów przerobionych plastycznie*. Część 3: *Skład chemiczny i rodzaje wyrobów*. 2009.
- POLAK J. 1991. *Cyclic plasticity and low cycle fatigue life of metals*. Materials Science Monographs, 63. *Problemy badań i eksploatacji techniki lotniczej*. T.2. Eds. J. Lewitowicz, J. Borgoń, W. Ząbkowicz. Wyd. ITWL, Warszawa.
- SIENIAWSKI J. 2002. *Rozwój metod projektowania i oceny mikrostruktury i właściwości materiałów konstrukcyjnych dla techniki lotniczej*. In: *Postępy nauki o materiałach i inżynierii materiałowej*. Ed. M. Hetmańczyk. Wydawnictwa Politechniki Śląskiej, Katowice.

